ACS APPLIED NANO MATERIALS

www.acsanm.org

Article

Phosphonated Polyetheramine-Coated Superparamagnetic Iron Oxide Nanoparticles for Inhibition of Oilfield Scale

Mohamed F. Mady,* Ali H. Karaly, and Malcolm A. Kelland

Cite This: *ACS Appl. Nano Mater.* 2023, 6, 6739–6750

Read Online

ACCESS | Metrics & More | Article Recommendations | Supporting Information

ABSTRACT: Oilfield scale is one of the significant problems in hydrocarbon production in the oil and gas industry. Many research groups have attempted to develop greener chemicals to meet environmental regulations. Magnetic nanoparticles are an intriguing technology due to their multiple properties, such as size effects, surface-to-volume ratio, magnetic separation, specificity, low toxicity, and the ability to control exposure and surface chemistry. In this project, we propose a new method to remove chemicals from the produced fluids by attaching the chemicals to superparamagnetic iron oxide nanoparticles (SPIONs), allowing a facile magnetic removal and reusing and recycling. In principle, the system is fully self-contained, and no chemicals or SPIONs are discharged, reducing the overall environmental footprint. We earlier reported synthesizing and using phosphonated polyetheramines (PPEAs) as environmentally friendly and potent scale inhibitors against carbonate and sulfate oilfield scales. Herein, we report the synthesis of superparamagnetic iron oxide nanoparticles (SPIONs) functionalized with biocompatible trisodium citrate (TSC) as a stabilizer agent to avoid crystal grain growth SPIONs using a coprecipitation approach. The resultant SPIONs-TSC was further functionalized with a partially linear phosphonated polyetheramine (PPEA), as green SI, via electrostatic interaction, affording highly monodisperse SPIONs-TSC-PPEA. The synthesized SPIONs-TSC-PPEA was thoroughly characterized via various spectroscopic and analytical techniques. Moreover, to validate the proof of concept of inhibition, recovering, and recycling SPIONs-based scale inhibitors, a series of static jar tests and high-pressure dynamic tube-blocking tests at 80 bar and 100 °C under oilfield conditions were conducted. The results showed that SPIONs-TSC-PPEA gave excellent inhibition performance against the gypsum scale even when recycled four times. In addition, the morphology of the gypsum scales in the absence and presence of SPIONs-TSC-PPEA was determined using scanning electron microscopy (SEM).

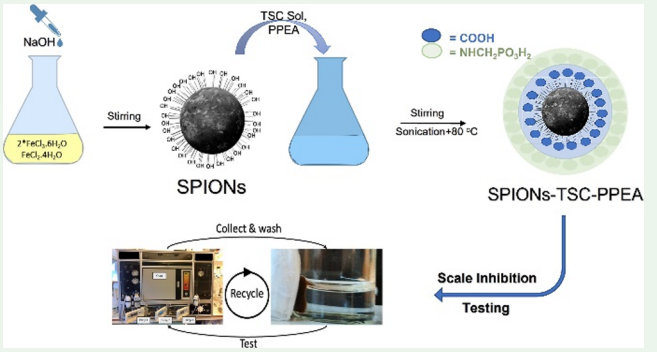

KEYWORDS: *superparamagnetic iron oxide nanoparticles, oilfield scale inhibition, phosphonated polyetheramines, zero waste, chemical recycling*

1. INTRODUCTION

Scale formation is the process of inorganic salt deposition from the aqueous phase because of salt saturation.[1] Scale can deposit on almost any surface. Once a scale layer is formed, it will gradually become thicker unless treated. Scale can block pore throats in the near-wellbore region or in the well itself, causing formation damage and loss of well productivity.[2] In general, scaling is a complex phenomenon and involves crystallization mechanisms.[3] Once the activity of cations and anions in the solution surpasses their saturation limit for a particular salt, the crystallization and following scale deposition can occur. Also, the kinetics of the reaction plays a vital role in the degree of scaling.[4] Both surface and bulk crystallization are the two mechanisms that will cause scale formation.[2,4] Figure S1 shows a typical oilfield scale formed in the pipeline.[5]

The most typical types of oilfield scales are calcium carbonate ($CaCO_3$) and sulfates of group II elements, for example, strontium (celestite, $SrSO_4$), calcium (gypsum, $CaSO_4.2H_2O$), and barium (barite, $BaSO_4$).[3] Barite, gypsum and calcite scales are the extreme scales in oilfield applications. So, it is imperative to tackle the problem of scale deposition wisely and quickly to increase the total revenue from the petroleum reservoir. In addition, the gypsum oilfield scale still causes several unforeseen issues in many oilfields.[5]

There is an urgent need to mitigate the scale formation for an economical and safe perspective in the petroleum industry. Scale control must be quick and non-damaging to the wellbore,

Received: February 1, 2023
Accepted: March 29, 2023
Published: April 11, 2023

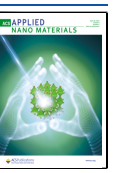

tubing, and petroleum reservoir. Conventional mechanical methods displayed an excellent treatment technique to remove the inorganic deposits in the wellbore tubular using abrasive jetting or milling. In addition, chemical treatment-based scale dissolution techniques (e.g., acid stimulation or chelating agents) are widely used for scale removal in the upstream oil and gas industry, mainly carbonate scaling. However, mechanical and chemical dissolution approaches showed drawbacks, such as high cost and corrosion issues.

Scale control using chemical inhibition treatment is optimal for maintaining petroleum reservoir productivity.[6] Scale inhibitors (SIs) are a branch of specialty water-soluble chemicals used to prevent or slow scale formation in water systems. SIs are the most common and applicable scale control technique, as it inhibits the nucleation of the crystal from the beginning.[6] There are two main ways of applying SIs in oilfield applications: squeeze treatment and continuous injection. In squeeze treatment, the SI is injected by a specific concentration into the well, retained on formation rocks, and then released during oil production to inhibit scale formation. In continuous injection, a small portion of the SI is added to the injection water with its minimum inhibitory concentration for scale formation.[7]

Most commercial SIs are polymeric and non-polymeric compounds containing functional inhibition groups such as phosphonate, carboxylate, and sulfonate groups. Organophosphorus compound-based SIs are widely used as potential SIs for various inorganic deposits in the upstream oil and gas industry. It is well known that the concentration of phosphonate-based SIs can be easily determined in water formation using several analytical and spectroscopic techniques. However, these classes showed several drawbacks, such as low biodegradability and various incompatibilities with the production system. Thus, several attempts have been investigated to develop more environmentally acceptable SIs containing phosphonate moiety (PO_3H_2).

The need for green oilfield production has grown considerably in the last two decades in light of our understanding of environmental issues, as determined by the Oslo and Paris Commission (OSPARCOM). Several attempts have been reported to develop environmentally friendly chemicals for oilfield applications. In the last 10 years, our Green and Sustainable Chemistry research group at the University of Stavanger has designed many biodegradable and non-toxic phosphonated SIs for oilfield applications. Figure S2 shows some selected environmentally acceptable SIs developed by our research group.[8,9] However, so far, greener chemicals suffer from low performance, high cost, and various incompatibilities with the production system. Therefore, there is an urgent need to develop a new way to avoid chemical pollution from oilfield operations.

Nanoscience has grown considerably in various industrial and medical applications. Due to their unique physical and chemical features, nanoparticles have recently been greatly interested in the upstream oil and gas industry.[10] Environmental nanoscience or nano-ecotoxicology has emerged in recent years, aiming to elucidate the toxicity potential of nanomaterials linked to their physicochemical characteristics. Magnetic nanoparticles (MNPs) have multiple interesting properties, such as size effects, surface-to-volume ratio, magnetic separation, specificity, low toxicity, and the ability to control exposure and surface chemistry.[11] MNPs, in particular, nano zero-valent iron, magnetite, and maghemite have sparked potential applications in medicine, molecular biology, and the remediation of polluted water.

Superparamagnetic iron oxide nanoparticles (SPIONs) (also known as superparamagnetic magnetite Fe_3O_4) is the most widely used in various medical and environmental application due to their high biocompatibility and low toxicity.[12] Many synthetic methods have been reported for SPIONs preparation. For example, coprecipitation, thermal decomposition, hydrothermal, microemulsion, sol−gel, ball milling, microwave irradiation, and ultrasonic irradiation are the most typical synthetic procedures. It is well known that the coprecipitation technique provides a simple and efficient synthetic process for obtaining high monodisperse SPIONs of controlled size and magnetic performance.[13] The surface area of the synthesized SPIONs via the coprecipitation method is vibrant with several active sites, which can be easily further functionalized with various functional moieties.[14] However, there is an urgent need to stabilize the SPIONs to avoid the formation of larger particles via aggregation and improve surface functionalization. There are several stabilizing agents used for improving the physicochemical characteristics of SPIONs.

Trisodium citrate (TSC) stabilizer has received significant attention due to its highly cost-effective, low toxicity, and unique physicochemical properties. It was reported that superparamagnetic iron oxide nanoparticles coated with trisodium citrate (SPIONs-TSC) provided a biocompatible water-soluble monodisperse composite for biomedical applications.[15]

The primary objective of this project is to investigate for the first time the use of revolutionary MNPs to prevent scale formation under oilfield conditions, using a simple, cost-effective method by attaching green chemicals to superparamagnetic iron oxide nanoparticles (SPIONs), allowing a facile magnetic removal, along with reuse and recycling. This method is unique as it will potentially give ZERO environmental impact from oilfield operations.

Early work showed that a series of environmentally friendly phosphonated polyetheramines (PPEAs) provided excellent scale inhibition performance for calcium carbonate and barium sulfate scales according to the Heidrun oilfield, Norwegian Sea, Norway.[16] In addition, these green PPEAs showed outstanding calcium compatibility up to 10,000 ppm Ca^{2+} ions and excellent thermal stability at 130 °C for 7 days. Do et al. have used the magnetic nanoparticles to coat them with SIs, however, with no attempts to recycle the used nanoparticles.[17] Herein, we report the synthesis of superparamagnetic iron oxide nanoparticles (SPIONs) functionalized with biocompatible trisodium citrate (TSC) as a stabilizer agent to avoid crystal grain growth SPIONs using a coprecipitation approach. The resultant SPIONs-TSC was further functionalized with a partially linear phosphonated polyetheramine (PPEA), as green SI, via electrostatic interaction, affording highly monodisperse SPIONs-TSC-PPEA.[18] Furthermore, this magnetic core-shell (SPIONs-TSC-PPEA) was evaluated for calcium sulfate scale (gypsum, $CaSO_4.2H_2O$) inhibition under static and dynamic oilfield conditions. This study will validate the proof of concept of recovering and recycling SPIONs-based scale inhibitors for the first time.

2. EXPERIMENTAL SECTION

2.1. Materials and Characterization. All chemicals and solvents were sourced from Tokyo Chemical Industry Co., Ltd., Sigma-Aldrich (Merck), VWR chemicals, and ACROS Organics and were of

https://doi.org/10.1021/acsanm.3c00445
ACS Appl. Nano Mater. 2023, 6, 6739−6750

Scheme 1. Schematic Representation of Synthesis Process of SPIONs-TSC-PPEA and Recycling

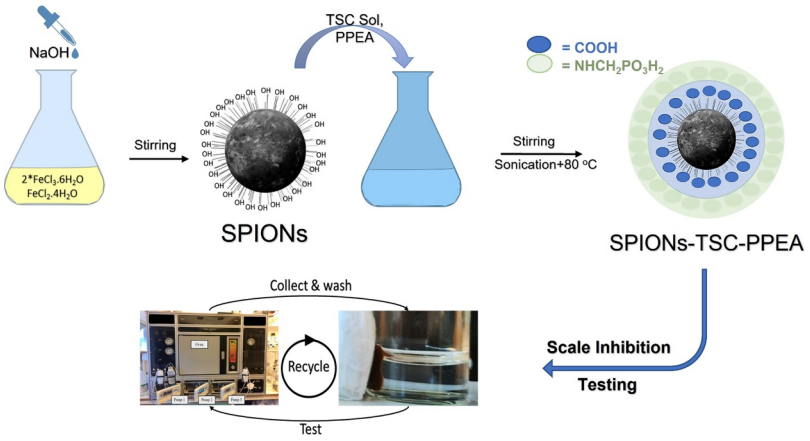

analytical grade. They were utilized as received without further modification unless otherwise described. Commercial scale inhibitors aminotrimethylenephosphonic acid (ATMP) and diethylenetriaminepentatakis(methylene phosphonic acid) (DTPMP) were obtained from Italmatch Chemicals S.p.A. Italy. Polyetheramine (EDR-176) was obtained from Huntsman Corp.

The following devices have been used; Z671797 IKA C-MAG HS hotplate stirrer, pH/mV/°C meter, bench, pHenomenal pH 1100 L VWR, PC 3001 VARIOpro EK Peltronic rotavap with RV 10 digital pro V Complete IKA, Branson Sonifier Digital Ultrasonic Cell Disruptor/Homogenizers, Bransonic ultrasonic cleaner, and Milli-Q water was obtained from ELGA PURELAB Option-R 7.

2.2. Preparation of Environmentally Friendly Phosphonated Polyetheramine Scale Inhibitor (PPEA). Partially linear phosphonated polyetheramine (**PPEA**) was synthesized via the Moedritzer-Irani reaction by reacting polyetheramine (**PEA**, molecular mass = 176) with phosphorous acid (H_3PO_3) and methanal (formaldehyde, HCHO) in the presence of a catalytic amount of hydrochloric acid (HCl), as shown in Figure S3.[16,19] The synthetic procedure of **PPEA** is as follows: In a two-neck round-bottom flask connected with a reflux condenser at 40 °C under nitrogen and the magnetic stirring bar were added linear polyetheramine PEA-176 (2 g, 1.00 equivalent), and phosphorus acid (1.88 g, 2.00 equivalent) in distilled water (10 mL). Then, hydrochloric acid (37%, 2.24 g, 2.00 equivalent) was added dropwise for ca. 30 min and allowed to heat stepwise from 40 to 60 °C under a nitrogen atmosphere. Then, methanal (37%, 1.86 g, 2.00 equivalent) was injected dropwise into the mixture solution using rubber cork over 30 min. The temperature of the reaction mixture was raised to 125 °C and heated under reflux for 24 h in the presence of nitrogen gas. The reaction solution was cooled and washed several times with diethyl ether using a separatory funnel. The washing solvent was removed using a rotary evaporator, affording an oily product (4.1 g). **PPEA** was used for the surface functionalization on SPIONs-TSC without further purifications.

2.3. Synthesis of Superparamagnetic Iron Oxide Nanoparticles (SPIONs) and Surface Functionalization. SPIONs synthesis and coating processes are illustrated in the following sections, as summarized in Scheme 1.

2.3.1. Synthesis of SPIONs. The magnetite Fe_3O_4 nanoparticles (SPIONs) were synthesized via a coprecipitation method of Fe^{2+} and Fe^{3+} ions under alkaline conditions.[14] In a two-necked Erlenmeyer flask fitted with a thermometer and funnel, a mixture of iron(III) chloride hexahydrate ($FeCl_3.6H_2O$, 14 g, 2.0 equivalent) and Iron(II) chloride tetrahydrate ($FeCl_2.4H_2O$, 5.15 g, 1 equivalent) was dissolved in 400 mL deoxygenated Milli-Q water. Under nitrogen flow, 36.25 g of ammonia solution 25% was dropwise into the flask with continuous stirring for 1 h. Finally, the overall solution was heated up to 70 °C to remove the excess unreacted ammonia solution and allowed to stir for 30 min. Then the precipitate was washed with DI water, collected by a magnet over 3 times, and allowed to dry using a rotary evaporator resulting in 5.99 g of SPIONs powder with a yield corresponding to 99.9%.

2.3.2. Synthesis of Trisodium Citrate-Coated SPIONs (SPIONs-TSC). SPIONs coating by citrate was carried out utilizing the electrostatic and steric effects between them, which enhances citrate conjugation to SPIONs and solution dispersion stability.[14] In a 500 mL beaker, trisodium citrate (15.62 g, 0.060 mol) was dissolved in 250 mL of DI water after degassing and deoxygenation. Then SPIONs (6.0 g, 0.025 mol) were added to the trisodium citrate solution, with pH adjustment of the overall pH of the solution to 6.5. The mixture was sonicated for 40 min, then moved to a two-necked round bottom flask and stirred under nitrogen flow for an hour, increasing the temperature to 80 °C. The particles were washed with DI water and collected by a magnet; the procedure was repeated 3 times and allowed to dry using a rotary evaporator resulting in 6.17 g of powder.

2.3.3. Preparation of Phosphonated Polyetheramine-Coated SPIONs-TSC (SPIONs-TSC-PPEA). Binding **PPEA** to citrate linker was done through the noncovalent bonding between secondary amines of the PPEA and carboxylate groups in the citrate.[20] In a 250 mL beaker, 0.132 g of PPEA was dissolved in 150 mL of degassed water. Then, 0.074 g of SPIONs-TSC were dispersed in the polymer solution using probe sonication for 2 min in probe sonication, followed by 60 min in bath sonication. The mixture was then moved to a two-necked round bottom flask and stirred under nitrogen flow for an hour at 80 °C. The particles were washed with DI water, collected by a magnet 3 times, and dried using a rotary evaporator resulting in 0.104 g of powder.

2.4. Characterization of Polymers, SPIONs, and Their Surface Functionalization. *2.4.1. XRD Measurement.* The crystallinity of the synthesized nanoparticles' crystallography and diffraction patterns were determined using X-Ray Diffraction (XRD) Bruker D8 Advance diffractometer at 40 kV, and 40 mA with 2θ is in the range of 10°−80° with a Cu K_α source with a wavelength of 1.5406 Å. All samples were ground into a fine powder using manual mortar, then placed and pressed into the specimen holder and put into the XRD Bruker D8 Advance diffractometer device.

2.4.2. Morphological Measurements. The morphology and size of the prepared nanoparticles were determined by scanning electron microscopy (SEM) and transmission electron microscopy (TEM) in bright field mode equipped with EDS (Energy Dispersive X-ray Spectrometer) with silicon drift detectors by SIGMA SEM Carl Zeiss NTS Ltd. and JEM-2100 Plus 200 kV and 0.19 nm spatial resolution (LaB6 electron gun), respectively.

2.4.3. Dynamic Light Scattering (DLS) and Zeta Potential Measurement. DLS and zeta potential of the synthesized particles have been assessed using Malvern Zetasizer nano series Ltd. The synthesized particles were dispersed in DI water at pH 7 and bath sonicated for 5 min before placing them in the cuvettes. The results were averaged over 10 measurements in triplicates.

2.4.4. TGA Measurement. Mettler Toledo TGA/DSC 3+ STARe System was used to examine the thermal stability of the synthesized

https://doi.org/10.1021/acsanm.3c00445
ACS Appl. Nano Mater. 2023, 6, 6739−6750

nanoparticles and polymers under a nitrogen atmosphere flow of 25 mL/min and temperature from 25 to 600 °C at a heating rate of 10 °C/min. All samples were vacuum dried in the rotavap at low pressure to eliminate any humidity and then premeasured onto platinum pans. The coating ratio can be determined by calculating the weight loss of the polymer and nanoparticles composite according to Dongargaonkar et al.[21]

2.4.5. Fourier-Transform Infrared (FTIR) Measurement. Infrared spectroscopy (IR) study was conducted using Agilent Cary 630 FT-IR spectrophotometer attached with an attenuated total reflectance (ATR). The samples were dried and placed onto the Zinc Selenide (ZnSe) crystal in transmission mode, swept from 400 to 4000 cm^{-1}, and absorption frequencies were represented in wave numbers (cm^{-1}).

2.4.6. Magnetization Measurement. To characterize the magnetic properties of the synthesized magnetic nanoparticles, the magnetization measurements were obtained using MPMS (SQUID VSM—Quantum Design) at 300 K. The magnetization properties of the synthesized SPIONs are crucial for their recyclability.

2.4.7. Nuclear Magnetic Resonance (NMR) Measurement. The structure of the synthesized polymer PPEA was confirmed by ^{1}H NMR and ^{31}P nuclear magnetic resonance (NMR) spectroscopy. The spectra were recorded on a 400 MHz Bruker NMR spectrometer, and the samples were dissolved in deuterium oxide (D_2O) solution for the ^{1}H NMR and ^{31}P NMR.

2.5. Testing of Scale Inhibition Performance. *2.5.1. Static Jar Test.* A static inhibition test has been conducted to determine the oilfield scale inhibition performance of the synthesized nanoparticles. The static inhibition test is standardized under the condition of NACE Standard TM0374-2007 protocol.[22] It requires the existence of the anion and cations solution with the tested chemical in several concentrations.[23] The composition of cationic and anionic brines related to the calcium sulfate scale (gypsum, $CaSO_4.2H_2O$) (1:1 ratio between formation water and seawater) was prepared as described in Table S1 by dissolving the respective salts in DI water.

In 50 mL Schott Duran glass bottles, the mixture of cationic and anionic brines (B1 and B2, respectively) with SIs samples were prepared at different concentrations of SI (100, 50, 20, 10, 5, 2, and 1 ppm) according to Table S2 by diluting a 1000 ppm stock solution of SI with pH around 4.5. The pH was adjusted to be 4.5−6 to mimic a typical petroleum reservoir. In addition to the SI samples, two additional blank bottles were prepared to behave as controls. Automated Thermo Fisher Scientific, USA, 100 μL, 1, and 10 mL pipettes were used to control the mentioned volumes accurately.

All the bottles with solution mixtures mentioned in Table S2 were prepared, mixed, closed tightly, and heated at 80 °C for 5 h according to the optimum time for scale growth, as presented in Figure S4.[24] Figures S5−S8 show the static inhibition test of SPIONs-TSC-PPEA, PPEA, and commercial SIs DTPMP, and ATMP, respectively, at different concentrations (1−100 ppm) before and after 5 h at 80 °C. After the reaction, the concentration of free calcium ions was determined by titration against ethylenediaminetetraacetic acid (EDTA) as a probe for SI efficacy according to the protocol given by ASTM D-511.[25]

The titration setup consisted of a 50 (±0.1) ml glass burette (Hirschmann, Germany) with a laboratory disc stirrer (VWR). Typically, 1 mL of each sample mixture was diluted to 50 mL using DI water in a conical flask with a magnet stirrer, and pH was adjusted to 12−13 by adding 100 μL of NaOH 50%. The mixtures were titrated in triplicates against 0.01 M EDTA using Murexide as an indicator; the color changed from pink to purple. The titrations were done in triplicates to confirm the reproducibility of the results. The standard deviation of the obtained results was in the range of 1−5%.

The calcium ions concentration was calculated using eq 1.

$$[Ca^{2+}](\text{ppm}) = \frac{V_{EDTA}(\text{mL}) \times [\text{EDTA}]\left(\frac{\text{mol}}{\text{L}}\right)}{V_S(\text{mL})} \times MWt_{Ca}\left(\frac{\text{mg}}{\text{mol}}\right) \quad (1)$$

where V_{EDTA} is the volume of the used EDTA in the titration, [EDTA] is the EDTA concentration, V_S is the volume of the sample used (50 mL), and MWt_{Ca} is the molecular weight of calcium (40,100 mg/mol).

The inhibition efficiency of SIs was then calculated based on the free Ca^{2+} ions. As the SI performs best when no precipitation reaction occurs, the Ca^{2+} is maximum. The inhibition % was calculated using eq 2.

$$\text{Inhibiton\%} = \frac{C_1 - C_o'}{C_1 - C_o} \quad (2)$$

where C_1 refers to the $[Ca^{2+}]$ in the sample after 5 h reaction, C_o' is the $[Ca^{2+}]$ in the blank after 5 h reaction, and C_o is the $[Ca^{2+}]$ in the blank before reaction.

The recyclability of the SPIONs-TSC-PPEA nanocomposite has been tested by recollecting the nanocomposite particles from a concentration of 100 ppm using a magnet from the side, as shown in Figure S9. The collected particles were washed three times with DI water, then sonicated for 10 min to remove any potential scale formation, recollected by a magnet from the side with a final wash using DI water, and left to dry in the rotary evaporator. After drying, the nanocomposite powder was weighed and resuspended to make another 100 ppm concentration, according to Table S2. The scale inhibition performance of the recycled SPIONs-TSC-PPEA nanocomposite was tested against gypsum scale under the same static harsh conditions. This process has been repeated five times representing five recycling cycles.

2.5.2. High-Pressure Dynamic Tube Blocking Test. The high-pressure dynamic tube blocking test is an efficient laboratory method to monitor the inhibition efficiency of SIs against different inorganic scales under conditions of pressure and temperature mimicking the environment of several industrial applications, including for oil and gas field applications.[9,16,26] The used dynamic tube blocking scale rig was manufactured by Scaled Solutions Ltd. (UK). The operation mimics the scale formation process inside the pipelines regarding pressure and temperature and measures the SIs' efficiency in inhibiting scale formation.

The rig's heart consists of three pumps of pumping power that reach a 10 mL/min rate through the 316 microbore coil. The coil is 3 m long, 1 mm inner diameter, and placed in the oven. Values of the differential in pressure across the coil can indicate the rate of scale formation. A computer compiles the differential results on an Excel file to plot the data to show the minimum inhibitor concentration (MIC) of the SIs. The tube of the rig is designed to withstand temperature and pressure up to 200 and 300 bar. The scale deposition is triggered to stop when the differential pressure jumps over 1 bar (14 psi).

The first pump is used to pump brine 1, containing the cations. The second pump has a switching valve connected to three inlets, brine 2 containing the anions, scale removing solution that consists of a high pH solution of tetrasodium ethylenediaminetetraacetate (Na_4EDTA 5 wt %, pH = 11−13) in Milli-Q water, and Water used for scale removal and cleaning, respectively. The third pump is used to pump the SI with a pH of around 4.5. Before each experiment, all the mentioned solutions were degassed using a water vacuum pump. The contents of three pumps were pumped to the coil at 100 °C and 80 bar, connected to software to record differential pressure.

The operation protocol was set to ensure the reproducibility of the results. Typically, the automated protocol would start with the blank test without the scale inhibitor to find the original failing time at 0 ppm of the SI. Then a series of 1-h reaction with the scale inhibitor in descending order of concentrations till it reaches the fail inhibitory concentration (FIC). A repeated test would initiate from the concentration before the FIC, called the MIC until it reaches the FIC again. Finally, the blank test at 0 ppm SI would be repeated.

In this study, the initial maximum concentration of the SI was 100 ppm and descended to be 50, 20, 10, 5, 2, and 1 ppm, or till it reached the FIC. The cleaning sequence will proceed when it comes to the FIC, and the reaction is stopped. Typically, 5 wt % of tetrasodium

https://doi.org/10.1021/acsanm.3c00445
ACS Appl. Nano Mater. 2023, 6, 6739−6750

ethylenediaminetetraacetate scale removal solution (Na_4EDTA) that had a pH between 12 and 13 is injected for 10 min to remove any formed calcium sulfate scale. Water is injected for another 10 min to clean the coil. For the SPIONs-TSC-PPEA study, an additional step of washing with acetic acid (10%) was added.

All the obtained results were transferred to Excel files and processed as schematic graphs of the minute scaling time against the differential pressure (psi) inside the stainless-steel coil.

3. RESULTS AND DISCUSSION

Synthesis of well-dispersed coated SPIONs to be used as a scale inhibitor can be challenging. As said by Lewis et al.[27] in a conference held in Vancouver, "colloidal hate buffers" emphasize the difficulties of having a stable colloid suspension in a buffer or a brine. This can be affiliated with the potential surface dependence on the salt concentration as well as the pH of the surrounding medium between the ions of the buffer and SPIONs surface, as it can reach zero at high salt concentrations (0.15 M and above) that leads to particles aggregation and formation damage to the SI.[28,29] To provide salt tolerance to the synthesized SPIONs, citrate coating layer was added due to its reductive and complex forming ability.[30] In addition to citrate stabilizing effects, its biodegradable properties qualify it as a better candidate than other linkers, such as silicon-based linkers.[31]

3.1. Polymer and Nanoparticles Synthesis. *3.1.1. Phosphonated Polyertheramine (PPEA) SI Synthesis.* Methylenephosphonate groups have been introduced to the polyetheramine structure backbone to act as an efficient green-scale inhibitor for oilfield applications.[16] The reaction process started with the amino groups of the PEA that were functionalized with methylenephosphonate via Moedritzer Irani reaction using phosphorous acid, hydrochloric acid, and formaldehyde in water as a benign solvent, affording PPEA in a high yield, as presented in Figure S3.[24] The phosphonation of polyertheramine has been verified by ^1H NMR and ^{31}P NMR, as shown in Figures S10 and S11, respectively. ^1H NMR of PPEA in D_2O displayed triplet signals at δ 1.97−2.00 ppm attributed to $-OC\underline{H}_2C\underline{H}_2-O-$, a doublet peak at δ 3.47−3.51 ppm that is related to the methylene addition (CH_2) in methylene phosphonate ($-N-C\underline{H}_2-PO_3H_2$), and a multiplet peaks at δ 3.54−3.60 ppm attributing to ($O-C\underline{H}_2C\underline{H}_2CH_2-N$) protons.[16] The ^{31}P NMR chemical shift of the phosphonate groups in the addition of methylene phosphonate ($-N-CH_2-\mathbf{PO_3H_2}$) showed a singlet peak at δ 22.44 ppm. Indeed, these results are in great agreement with similar phosponated PPEA in the open literature.[16] In addition, FTIR spectra of PPEA displayed a significant absorption band at 910 and 1081 cm^{-1} correlated to the vibrations of P−O, and the broad peak in the range of 2600 to 3300 cm^{-1} that can be attributed to the OH bending vibrations.[32] In addition, the IR peak around 2800 cm^{-1} can be related to the secondary amine, which further confirms the partially phosphonated PPEA structure, as shown in Figure 1.[33]

3.1.2. Fourier Transform Infrared (FTIR) Spectroscopy. FTIR spectroscopy has been conducted to confirm the TSC linker and PPEA polymer coating upon the SPIONs core, as shown in Figure 1. The FTIR of the SPIONs-TSC showed significant absorption bands at around 1400 and 1600 cm^{-1}, corresponding to a COO^- symmetric stretching and COO^- antisymmetric stretching.[34] The SPIONs-TSC-PPEA phosphonate absorption band for PPEA coating is at 1081 cm^{-1}, which is correlated to the asymmetric vibrations of P−O.[32] In addition, The FTIR spectra of SPIONs-TSC-PPEA displayed a significant broad peak in the range of 3200 to 3700 cm^{-1} can be attributed to the OH^{1-} bending vibrations.[32] Moreover, a remarkable reduction in the intensity of SPIONs-TSC-PPEA peaks at 1400 and 1600 cm^{-1} related to the carboxyl groups was found. The consumption of carboxyl groups can explain this to attach to the PPEA coat.[34] The coating process of TSC onto the SPIONs surface is believed to be done via reacting the reactive ≡Fe−OH groups at the SPIONs surface (≈ 5 sites/nm^2) with the carboxylate coat via multipoint inner and outer sphere complex in addition to hydrogen bonds.[29,30,35] The addition of PPEA SI as the active outer layer of the SPIONs was performed utilizing the ionic interaction between the protonated primary and secondary amines (NH_3^+ and NH_2^+, respectively) in the PPEA and the carboxylic groups in trisodium citrate (COO^-).[18,36]

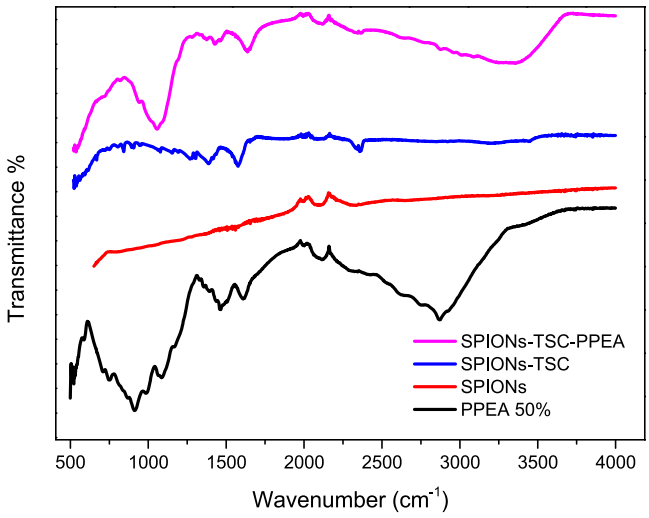

Figure 1. FTIR spectra of the prepared PPEA, SPIONs, SPIONs-TSC, and SPIONs-TSC-PPEA.

Furthermore, in the synthesis process, the nanoparticles are treated with excess polymer to ensure maximum coating. In the washing steps following, all the polymer not strongly linked to the nanocomposite through the combination of all mentioned bonding forces will fall out, and the rest of the strongly attached polymer will stick to the nanoparticle. This point is critical to the main goal of the study because if polymer leakage took place, it would defy the main reason for a zero-waste goal.

3.1.3. X-ray Diffraction (XRD). An XRD study has been conducted to reveal the crystal structure of SPIONs, SPIONs-TSC, and SPIONs-TSC-PPEA nanoparticles, as shown in Figure 2. The prominent obtained peaks are located at 2θ = 18.33°, 30.43°, 35.54°, 37.26°, 43.25°, 53.61°, 57.16°, 62.83°, 66.02°, 71.28°, 74.15°, and 75.25° that can be assigned to magnetite planes (1 1 0), (2 2 0), (3 1 1), (2 2 2), (4 0 0), (4 2 2), (5 1 1), (4 4 0), (5 3 1), (6 2 0), (5 3 3), and (6 2 2) respectively (RRUFF ID: R061111).[37] SPIONs-TSC-PPEA is more amorphous relative to other samples, which the existence of polymer surface coating can explain onto the crystalline core. However, there are no critical differences between the three samples confirming the magnetite core's stability and purity during synthesis procedures necessary for the recovery and recycling performance afterwards.

3.1.4. Thermogravimetric Analysis (TGA). To estimate the polymer coating weight percentage and thermal stability of the synthesized nanoparticles and polymer, TGA from 25 to 600

https://doi.org/10.1021/acsanm.3c00445
ACS Appl. Nano Mater. 2023, 6, 6739−6750

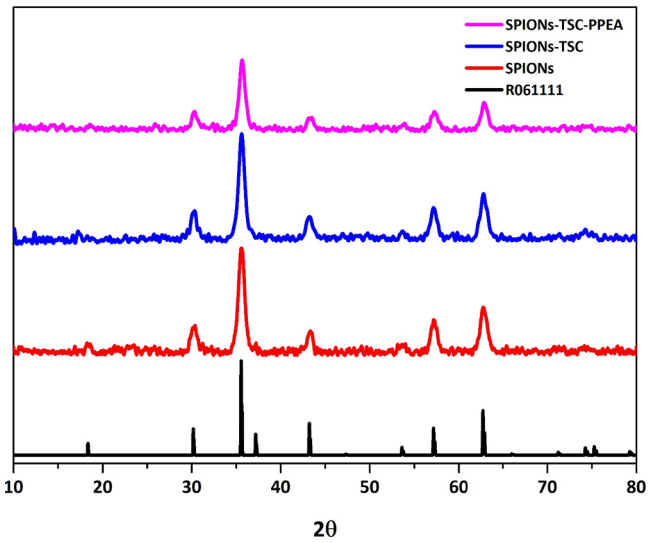

Figure 2. XRD patterns of SPION-TSC-PPEA, SPION-TSC, SPIONs, and reference with RRUFF ID: R061111.

°C in an inert nitrogen atmosphere has been conducted, as shown in Figures 3 and S12. The different curves between

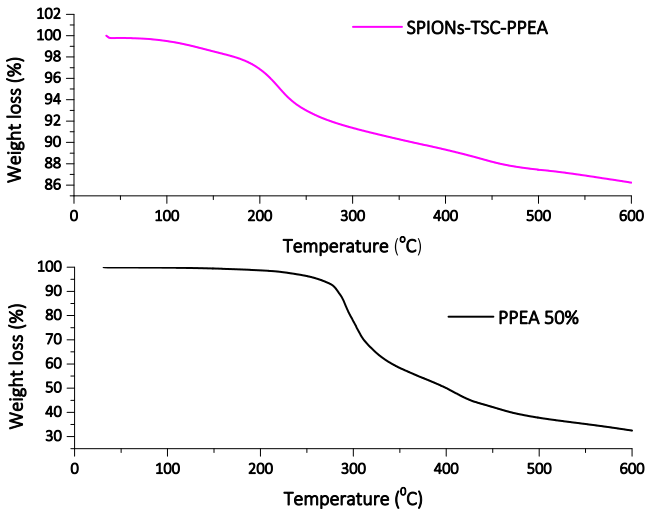

Figure 3. Schematic diagram of TGA of PPEA, SPIONs-TSC-PPEA SIs.

different tested samples result from the decomposition of the polymeric content of samples by the act of high temperatures. PPEA polymer experienced significant weight loss of more than 58% of its initial weight at approximately 200−600 °C. The synthesized nanoparticles SPIONs-TSC-PPEA lost over 23% of their initial mass percentage at about 150−550 °C, resulting mainly from the loss of the decomposition of the polymeric coat bonded to the nanoparticles' surface.[38] There is a limited water loss in samples due to samples pretreatment in the rotary evaporator under low pressure. In addition, the loss of the linker layer onto the SPINs-TSC nanoparticles is below 7% and assumed to be negligible, as shown in Figure S12. The difference between decomposition temperatures can be attributed to the effect of coating and enhanced surface area in the synthesized nanoparticles.[39] The coating percentage, according to Dongargaonkar et al., can be over 40% polymer of the nanocomposite total weight.[21]

3.1.5. Transmission Electron Microscopy (TEM) and Energy Dispersive X-ray Spectrometer (EDS). The morphology of the synthesized magnetic nanoparticles was investigated using Transmission Electron Microscopy (TEM), as shown in Figure 4. TEM shows the particle morphology to be quasi-spherical and has some tendency to aggregate in their solid dry state due to high surface tension.[40] The bare SPIONs appear to be monodisperse with an average diameter of around 10 nm. This range increases slightly upon coating with a citrate linker to about 11 nm. Finally, it reaches an average of 12 nm with a PPEA coating. The coating process did not change the main characteristics of the shape and uniformity of the particles. In addition, the polymer coat can be differentiated from the SPIONs core, as the core planes are visible with a laminar pattern, and the coat is more amorphous around the edges, as shown in Figure S13, which further confirms the coating's success. EDS reveals the sample composition related to the electron shells intensity of each element. As shown in Figure S14, the main elements related to our sample are iron, oxygen, phosphorus, and carbon. Copper is related to the sample holder's copper grid at the TEM instrument. Phosphorus and carbon presence can further confirm the surface coating of the TSC-PPEA polymer onto the SPIONs core.

3.1.6. Dynamic Light Scattering (DLS) and Zeta Potential. The high surface free energy of SPIONs colloidal solution caused by the high surface-to-volume ratio results in their kinetic instability.[41] It means that the nanosuspension of SPIONs will keep aggregate and increase its volume to decrease its surface-to-volume ratio, hence, its free energy. To reduce the high surface energy of SPIONs, the polymeric electrostatic coating can be applied to increase their stability.[29] Dynamic light scattering and zeta surface scattering studies were conducted for SPIONs-TSC-PPEA particles at different pH: 1, 5.5, and 13. These are summarized in Figures S15a,b, and Table S3. Solutions of each pH were left for a month and photographed, as shown in Figure S15c. At pH 1, the particles tend to aggregate as the zeta surface charge value is positive, indicating protonation of phosphonate function groups of PPEA surface coating, as shown in Figure S15a.[42]

Due to aggregation, the dynamic particle size tends to increase with a significant standard deviation (SD) value and a relatively high polydispersity index (PDI), as shown in Figure S15b. In addition, two peaks can be observed in the size distribution in Figure S16 representing aggregate formation due to the low charge shown in Figure S16b. Increasing pH to 5.5 to mimic the pH of the petroleum reservoir, the particles tend to have the highest dispersion with high zeta potential with a single peak, as shown in Figure S16d. The high dispersion can result from the deprotonation of PPEA surface function groups, resulting in the lowest and most stable PDI, smallest particle dynamic size, and highest monodispersity, as shown in Figure S16c. The solution managed to maintain a stable and clear dispersion for 5 weeks. They are shifting to a higher pH, with higher deprotonation results. This can result in two different deprotonations in surface coating, resulting in two zeta charge values of −42.and −24.7 mV, as shown in Figure S16f. In this case, attraction force increases between dispersed particles, which may be explained by the small absolute value of surface charge acting as a partial positive charge relative to the higher negative charge. This difference in charges leads to aggregation with time, as shown in Figure S16e.

https://doi.org/10.1021/acsanm.3c00445
ACS Appl. Nano Mater. 2023, 6, 6739−6750

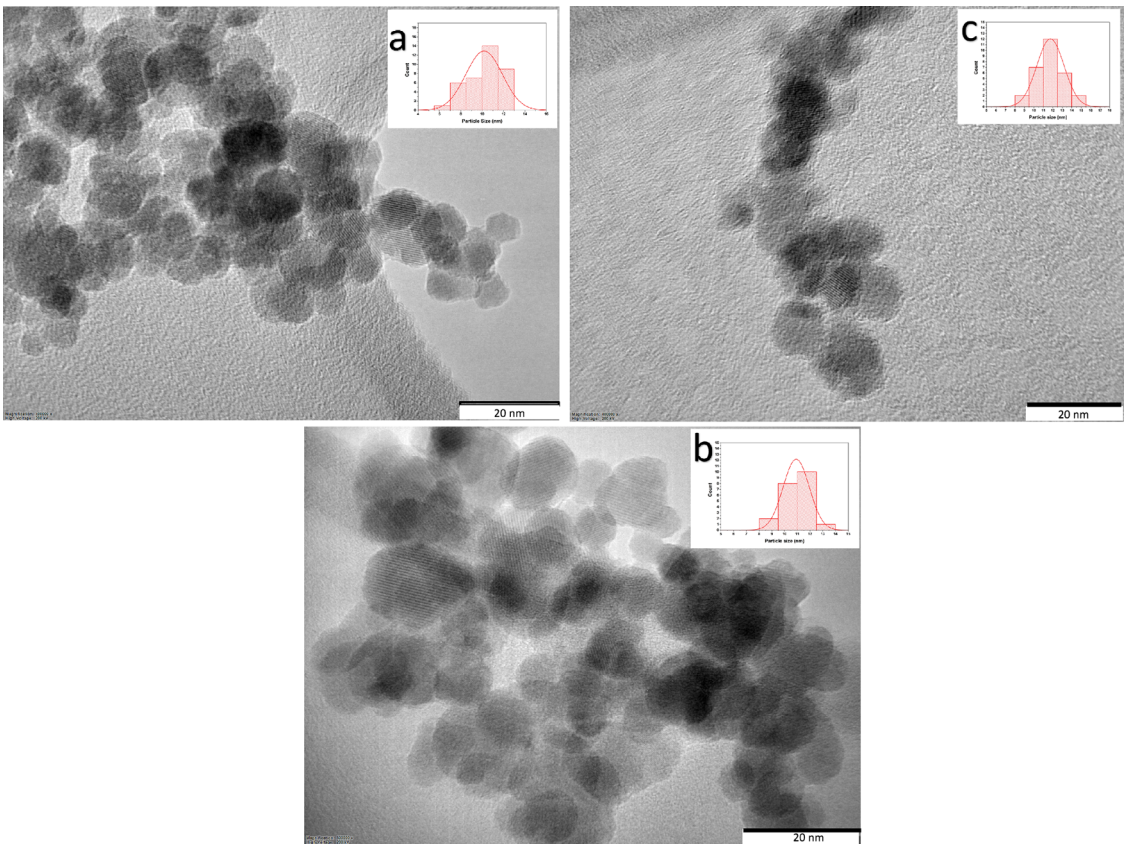

Figure 4. TEM images of the prepared particles; (a) SPIONs, (b) SPIONs-TSC, and (c) SPIONs-TSC-PPEA.

3.1.7. Magnetization Measurements. The magnetic measurement results showed high magnetization values for the synthesized SPIONs. Figure 5 and Table S4 show the main

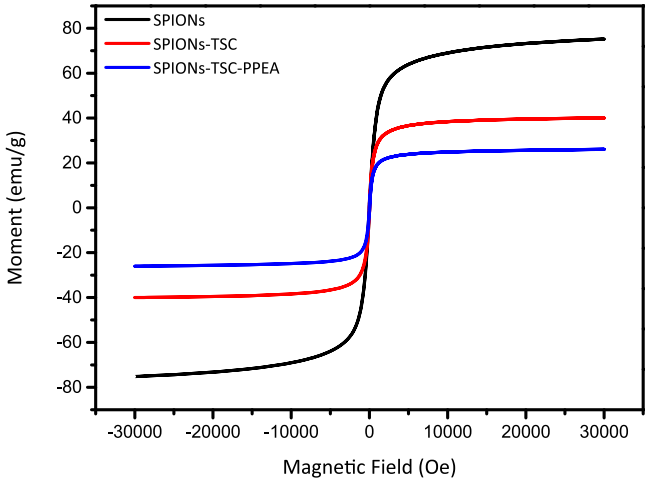

Figure 5. The hysteresis loops of SPIONs, SPIONs-TSC, and SPIONs-TSC-PPEA nanoparticles.

magnetization characteristics obtained from the hysteresis loops. These characteristic properties are magnetization saturation (M_s), coercivity field (H_c), and remnant magnetization (M_r). M_s value represents the highest value of the material magnetism that can be obtained under a high magnetic field, H_c is the value of applied magnetic field strength to recover the sample to the zero state of magnetization, and M_r is the value of magnetization at zero magnetic field.[43] The high values of M_s of SPIONs samples indicate their high magnetization capacity. However, the low values of H_c and M_r indicate their soft magnetism, meaning that each nanoparticle can be considered a single magnetic domain by itself. This feature showed the dispersibility of SPIONs samples in water after collection in the absence of a magnetic field that can prevent aggregation inside the pipelines.[43] From Table S4, it can be seen that the M_s values decrease with each coating layer from 75 emu/g in bare SPIONs to 40 emu/g in SPIONs-TSC to reach 26 emu/g in SPIONs-TSC-PPEA. This further confirms the successful coating onto the SPIONs surface, as the coating layer is non-magnetically susceptible and acts as a magnetic insulating barrier to the extent that it will not affect its recyclability.

3.2. Inhibition Testing of Scale Inhibitors. *3.2.1. Static Inhibition Test.* Commercial scale inhibitors such as ATMP and DTPMP have been tested against gypsum scale under static conditions in addition to PPEA and nanocomposite SPIONs-TSC-PPEA, as shown in Figures S5−S8 and 6. At low concentrations of SI, ATMP and DTPMP gave good inhibition performance against the gypsum scale. With higher concentrations of SI, ATMP inhibition performance decreased dramatically to reach 67% inhibition performance of gypsum scale at 100 ppm of SI, due to ATMP calcium incompatibility.[44] Then, the scale inhibition efficiency of both commercial SIs increased upon decreasing concentration to 76.92%, 82.69 ± 5.77%, and 98.08 ± 3.33% at 50, 20, and 10 ppm, respectively. DTPMP had a better performance at all screened concentrations of SI. It gave complete inhibition of gypsum scale at 100 ppm and continued to have acceptable

https://doi.org/10.1021/acsanm.3c00445
ACS Appl. Nano Mater. 2023, 6, 6739−6750

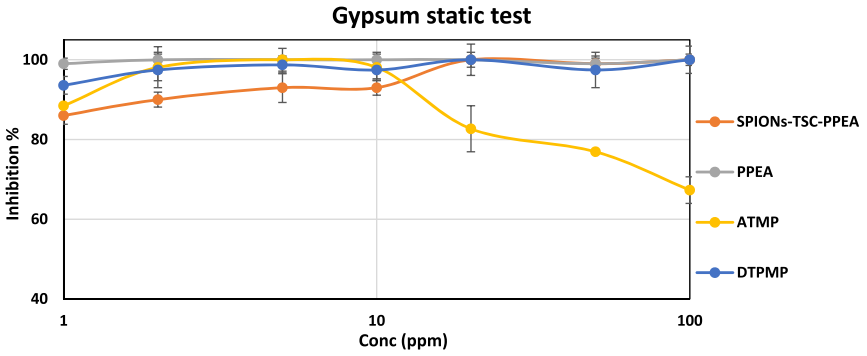

Figure 6. Gypsum inhibition performance of SIs.

performance at lower concentrations of SI to give 97.44 ± 4.44%, 100.00%, 97.44 ± 2.22%, 98.72 ± 2.22%, and 97.44 ± 4.44% at concentrations 50, 20, 10, 5, and 2 ppm of SI. It decreased to 88.6400% inhibition at the lowest concentration of 1 ppm of SI.

PPEA polymer had the best performance against the gypsum scale within all the screened concentrations of SI. It gave complete inhibition of gypsum scale from 100 to 1 ppm concentrations of SI. This performance compares well to the nanocomposite in the SPIONs-TSC-PPEA sample, as shown in Figure 6. Given that only 40% of the nanoparticle sample is active PPEA polymer, the composite gave total inhibition performance of gypsum scale at a high concentration of 100 to 20 ppm of SI. Then, the performance decreased with decreasing concentration, however with acceptable inhibition performance levels, to be 93 + 3.7%, 90 + 1.9%, and 86 + 2.2% at 10, 5, 2, and 1 ppm concentrations of SI.

It was well-known that most commercial aminomethylene phosphonates-based SIs are not compatible with calcium ions, leading to poor inhibition performance.[45] On the other hand, PPEA showed outstanding calcium compatibility properties, as discussed previously.[16] Also, the low biodegradation of ATMP and DTPMP makes the PPEA the best environmentally friendly candidate SI. The aerobic seawater biodegradation of PPEA reached 47% after 28 days.[16,46] The addition of SPIONs core to the PPEA polymer presents an added value of recovery of the polymer to ensure zero environmental waste with the possibility of recyclability. This is discussed in the following section.

3.2.1.1. Recyclability of SPIONs-TSC-PPEA. After a test in which SPIONs-TSC-PPEA showed complete inhibition of gypsum scale, the nanoparticles were recollected by a magnet placed on the side of the vessel and washed with DI water 3 times. They were then sonicated for 10 min, collected, and washed with DI water again, dried, redispersed, and tested for another 5 cycles, as shown in Figure S9. The efficiency of the recycled nanocomposite was acceptable in the first four cycles at around 80%, as shown in Figure 7. However, after the fifth cycle, the inhibition efficiency of SPIONs-TSC-PPEA against the gypsum scale dropped from 80 to approximately 50%. This drop can be explained by the growth of scale microcrystals within the SPIONs-TSC-PPEA nanoparticles that can block or hinder the active functional groups of the PPEA coat, as shown later in Figure 8.

3.2.1.2. Scanning Electron Microscopy (SEM) and Energy Dispersive X-ray Spectroscopy (EDS) Analysis. To understand the effect of SPIONs-TSC-PPEA SI against gypsum scale, an SEM study was conducted for gypsum scale formed (1) without the addition of SI, (2) without SPIONs-TSC-PPEA, and (3) in the presence of SPIONs-TSC-PPEA after 5 cycles. First, SEM micrographs of the gypsum scale formed without SI revealed the crystalline structure to be mostly monoclinic, as shown in Figure S17, which agrees with the literature.[47] Gypsum crystals are also known to be long, reaching several millimeters, as shown in Figure S17a. In addition, synthesized gypsum sulfate crystals are also known to have sharp edges like needles, which agrees with Figure S17b.[48] Moreover, the SEM analysis showed that the morphology of SPIONs-TSC-PPEA nanocomposite was monodisperse without any aggregation, as shown in Figure S18.

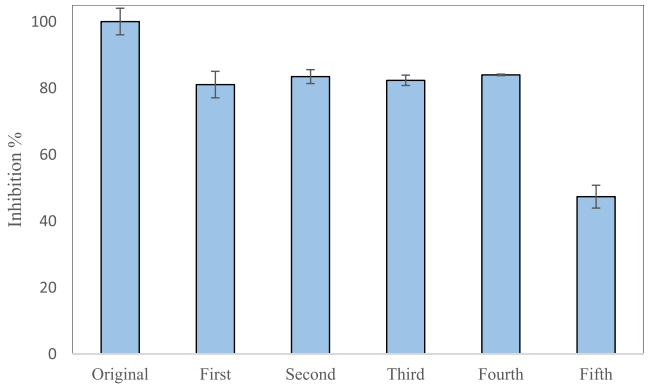

Figure 7. Recycling static inhibition test of SPIONs-TSC-PPEA against the gypsum scale.

The effect of SPIONs-TSC-PPEA as an SI against the gypsum scale can be shown in Figures S19 and 8. The inhibition efficiency of the recycled magnetic particles began to decrease with further cycles, as shown in Figure S19. After the fifth cycle, the particle morphology was also examined using SEM. The particles appear monodispersed; however, the originally long gypsum crystals in a needle-like shape could not be formed. As shown in Figure S19a, small fractions of the scale in a distorted form as a rod shape other than its original long crystals can be formed in low concentrations of the nanocomposite, which have a negligible effect, as shown in Figure S19b.

It was found that the SEM image displayed short threads after five cycles of static test, as shown in Figure 8a. In addition, the shape of the crystal is subjected to change upon the effect of SI.[49] It can be seen in Figure 8b that rod-shaped crystals are present.

To be certain about the type of scale formed after the fifth cycle of SPIONs-TSC-PPEA, EDS analysis was carried out, as shown in Figure 8c. The main elements presented in the EDS

https://doi.org/10.1021/acsanm.3c00445
ACS Appl. Nano Mater. 2023, 6, 6739−6750

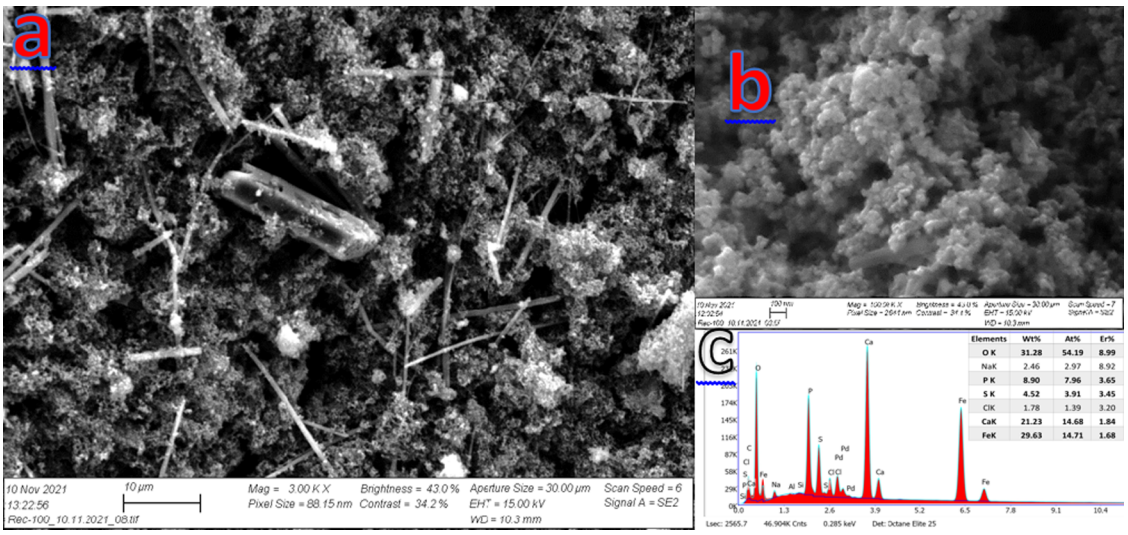

Figure 8. SEM of SPIONs-TSC-PPEA after 5th cycle at; (a) 10 μm, (b) 100 nm, and (c) EDS chart of part a.

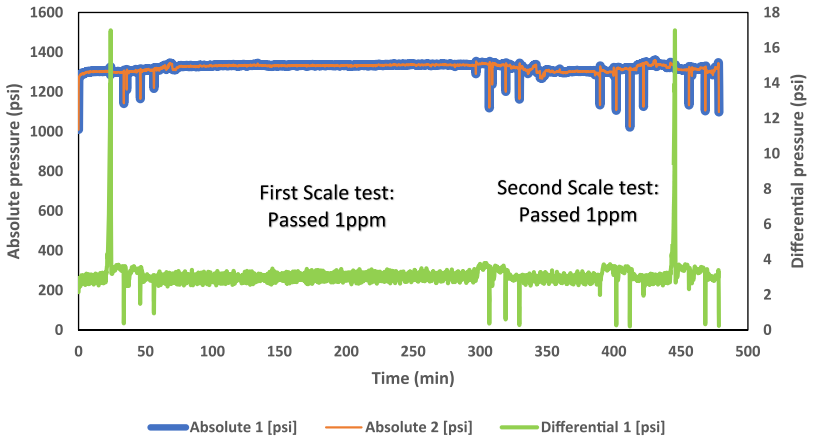

Figure 9. Graphical results of the high-pressure dynamic tube blocking test for SPIONs-TSC-PPEA against the gypsum scale.

analysis are oxygen, iron, calcium, phosphorus, and sulfur. Iron, oxygen, and phosphorus can represent the SPIONs-TSC-PPEA SI. Calcium, oxygen, and sulfur can represent the gypsum scale ($CaSO_4$). Some traces of other elements can be seen, such as palladium, caused by Pd metal coating, and NaCl traces of salt, which could have originated from the brine composition. Carbon is absent in the EDS analysis because it was included in the background due to its presence in the carbon tape on the sample holder.

3.2.1.3. Zero Marine Environment Test. Zero marine discharge of SIs is one of the main goals of the SPIONs-TSC-PPEA SI if used offshore. After applying our smart nanocomposite-based SI using the static test, the nanocomposite particles will be collected by a magnet. However, there is a possibility of the coat leakage or detachment from the SPIONs core and causing marine environmental waste if applied offshore. So, to claim that the nanocomposite SI causes zero environmental waste, we need to ensure no polymeric leakage after application. Therefore, after the static inhibition test, a 100-ppm sample of SPIONs-TSC-PPEA was collected by a magnet, as shown in Figure S9, and two drops of the remaining brine solution were tested by ^{1}H, and ^{31}P NMR spectroscopy, as shown in Figure S20. The test analyses confirmed the absence of organic residues in the brine solution after the test and after recollecting the SPIONs-TSC-PPEA nanocomposite.

3.2.2. High-Pressure Dynamic Tube Blocking Test. The dynamic scale loop inhibition performance test was conducted as further confirmation of the scale inhibition ability of the SPIONs-TSC-PPEA. The pH of the test solution was adjusted to be around 4.5 to match the static conditions.[16,50]

Figure 9 shows the graphical plot of SPIONs-TSC-PPEA against the gypsum scale using the dynamic tube blocking test at 100 °C and 80 bar. Further test information is given in Figures S21−S23. The first stage of the test is to run a blank test without inhibitor to determine the standard scaling time of the gypsum scale. This blank test and the repeat blank test gave similar results of 24 min (0−24 min on the graph) and 28 min (422−450 min on the chart). As shown in Figure 9, the SPIONs-TSC-PPEA SI passed the test with the lowest concentration of 1 ppm injected. This was confirmed in the repeat test, also shown in Figure 9.

The static inhibition test and high-pressure dynamic tube blocking test results with SPIONs-TSC-PPEA do not match, but the conditions vary in several respects. In the static test, 20 ppm is required for complete gypsum inhibition over 24 h at 80 °C. The dynamic test measures the scaling over 1 h at 100 °C. The environment at the static scale inhibition test is

https://doi.org/10.1021/acsanm.3c00445
ACS Appl. Nano Mater. 2023, 6, 6739−6750

harsher due to the higher ability of scale formation in this test.[51]

4. CONCLUSIONS

The main conclusions from this study are as follows:

1. A partially phosphonated polyetheramine PPEA was shown to give excellent gypsum scale inhibition. PEAA also exhibited excellent biodegradation properties and calcium compatibility.
2. Superparamagnetic iron oxide nanoparticles (SPIONs) functionalized with biocompatible trisodium citrate (TSC) were further functionalized with PPE, affording highly monodisperse SPIONs-TSC-PPEA. Particle size was 12 nm (average), and the PPEA coating percentage was over 40 wt % polymer. This composite was highly mono-dispersed, appeared as a water-soluble solution to the naked eye and was characterized by various techniques.
3. SPIONs-TSC-PPEA gave excellent inhibition performance calcium sulfate (gypsum) under both static and dynamic conditions. For example, no gypsum scale was formed at 1 ppm of SPIONs-TSC-PPEA-based SI under dynamic conditions at 100 °C and 80 bar using a high-pressure dynamic tube-blocking rig.
4. The scale inhibition efficiency of recycled SPIONs-TSC-PPEA against gypsum scale was confirmed under harsh static conditions. The efficiency of the recycled nanocomposite was acceptable (ca. 80%) in the first four cycles but dropped to around 50% in the fifth cycle. This drop can be explained by the growth of scale microcrystals within the SPIONs-TSC-PPEA nanoparticles that can block or hinder the active functional groups. The composite is thermally stable at harsh static test conditions without any coat leakage or detachment from the SPIONs core.
5. The morphology of the formed gypsum scale in the presence of SPIONs-TSC-PPEA nanocomposite was distorted from sharp needles to a rod shape without any aggregation. SEM images of the recycled SPIONs-TSC-PPEA displayed short threads after five cycles of static tests.
6. Further studies are needed to investigate the mechanism of the nanocomposite decreasing efficiency over cycles and its ability to perform in harsher conditions.

This study validated the proof of concept of recovering and recycling SPIONs for oilfield scale management for the first time. We are currently studying the performance of SPIONs-TSC-PPEA against other scales as well as their calcium compatibility and toxicity and of SPIONs-TSC-PPEA. We are also investigating methods to improve the recyclability of scale inhibitor-coated SPIONs without any loss of inhibition performance.

■ ASSOCIATED CONTENT

Supporting Information

The Supporting Information is available free of charge at https://pubs.acs.org/doi/10.1021/acsanm.3c00445.

Figure S1: Pipeline contaminated with oilfield scale, Figure S2: Some of the environmentally acceptable phosphonated SIs were developed by our research group, Figure S3: General scheme of the synthesis of phosphonated polyetheramines (PPEA), Figure S4: Duration test results for static test, Figures S5−S8: Static inhibition test of different concentrations of PPEA, DTPMP, ATMP, and SPIONs-TSC-PPEA, Figure S9: Mechanism of nanocomposite collection for recycling, Figures S10 and S11: ^{1}H, and ^{31}P NMR spectra of PPEA, Figure S12: Schematic diagram of TGA of SPIONs-TSC, Figures S13 and S14: TEM, and EDS of SPIONs-TSC-PPEA, Figure S15: Zeta potential and Size distribution of SPIONs-TSC-PPEA, Figure S16: Zeta potential and Size distribution of SPIONs-TSC-PPEA, Figure S17: SEM images of Gypsum scale, Figures S18 and S19: SEM images of SPIONs-TSC-PPEA before and after static test, Figure S20: ^{1}H, and ^{31}P NMR of free SPIONs-TSC-PPEA, Figures: S21−S23: High-pressure dynamic tube blocking test for PPEA, DTPMP, and ATMP, Table S1: Composition of brine for gypsum scaling, Table S2: Solution doses for static performance tests of SIs, Table S3: DLS study of SPIONs-TSC-PPEA at different pH values, Table S4: Magnetic properties of the SPIONs, SPIONs-TSC, and SPIONs-TSC-PPEA nanoparticles (PDF)

■ AUTHOR INFORMATION

Corresponding Author

Mohamed F. Mady − *Department of Chemistry and Earth Sciences, College of Arts and Sciences, Qatar University, Doha 2713, Qatar; Department of Chemistry, Bioscience and Environmental Engineering, Faculty of Science and Technology, University of Stavanger, Stavanger N-4036, Norway;* orcid.org/0000-0002-4636-0066; Email: mmady@qu.edu.qa

Authors

Ali H. Karaly − *Department of Chemistry, Bioscience and Environmental Engineering, Faculty of Science and Technology, University of Stavanger, Stavanger N-4036, Norway;* orcid.org/0000-0002-1711-5862

Malcolm A. Kelland − *Department of Chemistry, Bioscience and Environmental Engineering, Faculty of Science and Technology, University of Stavanger, Stavanger N-4036, Norway;* orcid.org/0000-0003-2295-5804

Complete contact information is available at: https://pubs.acs.org/10.1021/acsanm.3c00445

Author Contributions

Conceptualization, M.F.M.; experimental work, A.H.K.; supervision M.F.M. and M.A.K.; writing-original draft preparation, M.F.M., M.A.K., and A.H.K. All authors have read and agreed to the published version of the manuscript. M.F.M. and A.H.K. contributed equally to writing the manuscript.

Notes

The authors declare no competing financial interest.

■ ACKNOWLEDGMENTS

Financial support from the Research Council of Norway for Green Production Chemistry-Based Nanotechnology through the project PETROMAKS 2 program/research project no. 300754. We thank the Research Council of Norway (RCN), and the University of Stavanger for the financial support for A.H.K. under the RCN Ph.D. fellowship grant (fellowship no. 300754-02).

REFERENCES

(1) Sallis, J.; Juckes, W.; Anderson, M.; Amjad, Z. Phosphocitrate-Potential to influence Deposition of Scaling ions and Corrosion. *Miner. Scale Inhib.* **1995**, 87−98.

(2) Frenier, W. W.; Ziauddin, M. *Formation, removal, and inhibition of inorganic scale in the oilfield environment*; Society of Petroleum Engineers Richardson: TX, 2008.

(3) Kelland, M. A. *Production chemicals for the oil and gas industry*; CRC Press, 2016.

(4) Amjad, Z. *The science and technology of industrial water treatment*; CRC Press (Taylor & Francis Group): Boca Raton, FL, 2010.

(5) Mady, M. F.; Kelland, M. A. Review of Nanotechnology Impacts on Oilfield Scale Management. *ACS Appl. Nano Mater.* **2020**, *3*, 7343−7364.

(6) Olajire, A. A. A review of oilfield scale management technology for oil and gas production. *J. Pet. Sci. Eng.* **2015**, *135*, 723−737.

(7) Vazquez, O.; Fursov, I.; Mackay, E. Automatic optimization of oilfield scale inhibitor squeeze treatment designs. *J. Pet. Sci. Eng.* **2016**, *147*, 302−307.

(8) (a) Mady, M. F.; Abdel-Azeim, S.; Kelland, M. A. Investigation of the Antiscaling Performance of Phosphonated Chitosan for Upstream Petroleum Industry Application. *ACS Sustainable Chem. Eng.* **2021**, *9*, 16494−16505. (b) Lei, W.; Wang, F.-Y.; Xia, M.-Z.; Wang, F. Synthesis and its scale inhibition effect of green scale inhibitor polyepoxysuccinic acid. *J. Chem. Ind. Eng.* **2006**, *57*, 2207.

(9) Mady, M. F.; Rehman, A.; Kelland, M. A. Synthesis and Study of Modified Polyaspartic Acid Coupled Phosphonate and Sulfonate Moieties As Green Oilfield Scale Inhibitors. *Ind. Eng. Chem. Res.* **2021**, *60*, 8331−8339.

(10) Boul, P. J.; Ajayan, P. M. Nanotechnology Research and Development in Upstream Oil and Gas. *Energy Technol.* **2020**, *8*, No. 1901216.

(11) Akbarzadeh, A.; Samiei, M.; Davaran, S. Magnetic nanoparticles: preparation, physical properties, and applications in biomedicine. *Nanoscale Res. Lett.* **2012**, *7*, 144.

(12) (a) Assa, F.; Jafarizadeh-Malmiri, H.; Ajamein, H.; Anarjan, N.; Vaghari, H.; Sayyar, Z.; Berenjian, A. A biotechnological perspective on the application of iron oxide nanoparticles. *Nano Res.* **2016**, *9*, 2203−2225. (b) Farjadian, F.; Moradi, S.; Hosseini, M. Thin chitosan films containing super-paramagnetic nanoparticles with contrasting capability in magnetic resonance imaging. *J. Mater. Sci.: Mater. Med.* **2017**, *28*, 47.

(13) Yusuf, M. S.; Rahmasari, R. Synthesis Processing Condition Optimization of Citrate Stabilized Superparamagnetic Iron Oxide Nanoparticles using Direct Co-Precipitation Method. *Biomed. Pharmacol. J.* **2021**, *14*, 1533−1542.

(14) Mary, A. R.; Narayanan, T.; Sunny, V.; Sakthikumar, D.; Yoshida, Y.; Joy, P.; Anantharaman, M. Synthesis of bio-compatible spion−based aqueous ferrofluids and evaluation of radiofrequency power loss for magnetic hyperthermia. *Nanoscale Res. Lett.* **2010**, *5*, 1706−1711.

(15) Shen, L.-H.; Bao, J.-F.; Wang, D.; Wang, Y.-X.; Chen, Z.-W.; Ren, L.; Zhou, X.; Ke, X.-B.; Chen, M.; Yang, A.-Q. One-step synthesis of monodisperse, water-soluble ultra-small Fe_3O_4 nanoparticles for potential bio-application. *Nanoscale* **2013**, *5*, 2133−2141.

(16) Mady, M. F.; Bayat, P.; Kelland, M. A. Environmentally Friendly Phosphonated Polyetheramine Scale Inhibitors—Excellent Calcium Compatibility for Oilfield Applications. *Ind. Eng. Chem. Res.* **2020**, *59*, 9808−9818.

(17) Do, B. P. H.; Nguyen, B. D.; Nguyen, H. D.; Nguyen, P. T. Synthesis of magnetic composite nanoparticles enveloped in copolymers specified for scale inhibition application. *Adv. Nat. Sci: Nanosci. Nanotechnol.* **2013**, *4*, No. 045016.

(18) Khouri, J.; Penlidis, A.; Moresoli, C. Viscoelastic properties of crosslinked chitosan films. *Processes* **2019**, *7*, 157.

(19) Moedritzer, K.; Irani, R. R. The direct synthesis of α-aminomethylphosphonic acids. Mannich-type reactions with orthophosphorous acid. *J. Org. Chem.* **1966**, *31*, 1603−1607.

(20) (a) Zhuang, L.; Zhi, X.; Du, B.; Yuan, S. Preparation of elastic and antibacterial chitosan−citric membranes with high oxygen barrier ability by in situ cross-linking. *ACS Omega* **2020**, *5*, 1086−1097. (b) Hao, L.; Yegin, C.; Talari, J. V.; Oh, J. K.; Zhang, M.; Sari, M. M.; Zhang, L.; Min, Y.; Akbulut, M.; Jiang, B. Thermo-responsive gels based on supramolecular assembly of an amidoamine and citric acid. *Soft Matter* **2018**, *14*, 432−439.

(21) Dongargaonkar, A. A.; Clogston, J. D. Quantitation of surface coating on nanoparticles using thermogravimetric analysis. In *Characterization of Nanoparticles Intended for Drug Delivery*, Springer, 2018; pp 57−63.

(22) NACE TM0374-HD2001-SG *Laboratory screening tests to determine the ability of scale inhibitors to prevent the precipitation of calcium sulfate and calcium carbonate from solution (for oil and gas production systems)*; National Association of Corrosion Engineers, 2007.

(23) Oshchepkov, M.; Golovesov, V.; Ryabova, A.; Frolova, S.; Tkachenko, S.; Kamagurov, S.; Rudakova, G.; Popov, K. Synthesis and visualization of a novel fluorescent-tagged polymeric antiscalant during gypsum crystallization in combination with bisphosphonate fluorophore. *Crystals* **2020**, *10*, 992.

(24) Mady, M. F.; Ortega, R.; Kelland, M. A. Exploring Modified Alendronic Acid as a New Inhibitor for Calcium-Based Oilfield Scales. *Energy Fuels* **2022**, *36*, 1863−1873.

(25) Machette, M. *Calcium and magnesium*; US Geological Survey Bulletin, 1983; Vol. *1648−1654*; pp 30.

(26) (a) Mady, M. F.; Kelland, M. A. Study on various readily available proteins as new green scale inhibitors for oilfield scale control. *Energy Fuels* **2017**, *31*, 5940−5947. (b) Mady, M. F.; Malmin, H.; Kelland, M. A. Sulfonated Nonpolymeric Aminophosphonate Scale Inhibitors—Improving the Compatibility and Biodegradability. *Energy Fuels* **2019**, *33*, 6197−6204.

(27) Lewis, J. Superparamagnetic iron oxides, from the lab to approval. In *11th Int. Conf. on the Scientific and Clinical Applications of Magnetic Carriers*, Vancouver, Canada, 2016; p Invited Talk 6.

(28) Hunter, R. *Foundations of colloid science*; Clarendon Press: Oxford, U.K., 1989; Vol. *1*.

(29) Tombácz, E.; Farkas, K.; Földesi, I.; Szekeres, M.; Illés, E.; Tóth, I. Y.; Nesztor, D.; Szabó, T. Polyelectrolyte coating on superparamagnetic iron oxide nanoparticles as interface between magnetic core and biorelevant media. *Interface Focus* **2016**, *6*, No. 20160068.

(30) Szekeres, M.; Tóth, I. Y.; Illés, E.; Hajdú, A.; Zupkó, I.; Farkas, K.; Oszlánczi, G.; Tiszlavicz, L.; Tombácz, E. Chemical and colloidal stability of carboxylated core-shell magnetite nanoparticles designed for biomedical applications. *Int. J. Mol. Sci.* **2013**, *14*, 14550−14574.

(31) (a) Gyawali, D.; Nair, P.; Zhang, Y.; Tran, R. T.; Zhang, C.; Samchukov, M.; Makarov, M.; Kim, H. K.; Yang, J. Citric acid-derived in situ crosslinkable biodegradable polymers for cell delivery. *Biomaterials* **2010**, *31*, 9092−9105. (b) He, Q.; Shi, J.; Zhu, M.; Chen, Y.; Chen, F. The three-stage in vitro degradation behavior of mesoporous silica in simulated body fluid. *Microporous Mesoporous Mater.* **2010**, *131*, 314−320.

(32) Giri, A.; Makhal, A.; Ghosh, B.; Raychaudhuri, A.; Pal, S. K. Functionalization of manganite nanoparticles and their interaction with biologically relevant small ligands: Picosecond time-resolved FRET studies. *Nanoscale* **2010**, *2*, 2704−2709.

(33) Vreugdenhil, A.; Balbyshev, V.; Donley, M. Nanostructured silicon sol-gel surface treatments for Al 2024-T3 protection. *J. Coat. Technol.* **2001**, *73*, 35−43.

(34) Zou, X.; Ying, E.; Dong, S. Seed-mediated synthesis of branched gold nanoparticles with the assistance of citrate and their surface-enhanced Raman scattering properties. *Nanotechnology* **2006**, *17*, 4758.

(35) (a) Hajdú, A.; Szekeres, M.; Tóth, I. Y.; Bauer, R. A.; Mihály, J.; Zupkó, I.; Tombácz, E. Enhanced stability of polyacrylate-coated magnetite nanoparticles in biorelevant media. *Colloids Surf., B* **2012**, *94*, 242−249. (b) Tóth, I. Y.; Illés, E.; Bauer, R. A.; Nesztor, D.; Szekeres, M.; Zupkó, I.; Tombácz, E. Designed polyelectrolyte shell

https://doi.org/10.1021/acsanm.3c00445
ACS Appl. Nano Mater. 2023, 6, 6739−6750

on magnetite nanocore for dilution-resistant biocompatible magnetic fluids. *Langmuir* **2012**, *28*, 16638−16646.
(36) Mohammad-Beigi, H.; Yaghmaei, S.; Roostaazad, R.; Arpanaei, A. Comparison of different strategies for the assembly of gold colloids onto Fe_3O_4@SiO_2 nanocomposite particles. *Phys. E* **2013**, *49*, 30−38.
(37) Lafuente, B.; Downs, R. T.; Yang, H.; Stone, N. 1. The power of databases: The RRUFF project. In *Highlights in mineralogical crystallography*; De Gruyter (O), 2015; pp 1−30.
(38) Cheng, C. M.; Wen, Y. H.; Xu, X. F.; Gu, H. C. Tunable synthesis of carboxyl-functionalized magnetite nanocrystal clusters with uniform size. *J. Mater. Chem.* **2009**, *19*, 8782−8788.
(39) Ziegler-Borowska, M.; Chelminiak, D.; Kaczmarek, H. Thermal stability of magnetic nanoparticles coated by blends of modified chitosan and poly(quaternary ammonium) salt. *J. Therm. Anal. Calorim.* **2015**, *119*, 499−506.
(40) Khalkhali, M.; Rostamizadeh, K.; Sadighian, S.; Khoeini, F.; Naghibi, M.; Hamidi, M. The impact of polymer coatings on magnetite nanoparticles performance as MRI contrast agents: a comparative study. *Daru* **2015**, *23*, 45. From NLM Medline
(41) (a) Zhao, X.; Liu, W.; Cai, Z. Q.; Han, B.; Qian, T. W.; Zhao, D. Y. An overview of preparation and applications of stabilized zero-valent iron nanoparticles for soil and groundwater remediation. *Water Res.* **2016**, *100*, 245−266. (b) Mondal, K.; Jegadeesan, G.; Lalvani, S. B. Removal of selenate by Fe and NiFe nanosized particles. *Ind. Eng. Chem. Res.* **2004**, *43*, 4922−4934. (c) Shi, R.; Ow, H.; Cox, J. R.; Kmetz, A. A.; Chen, H. Optimizing Colloidal Stability and Transport of Polysaccharide-Coated Magnetic Nanoparticles for Reservoir Management: Effects of Ion Specificity. *Front. Nanotechnol.* **2022**, *4*, No. 864644.
(42) Liu, X.; Mäki-Arvela, P.; Aho, A.; Vajglova, Z.; Gun'ko, V. M.; Heinmaa, I.; Kumar, N.; Eränen, K.; Salmi, T.; Murzin, D. Y. Zeta potential of beta zeolites: Influence of structure, acidity, pH, temperature and concentration. *Molecules* **2018**, *23*, 946.
(43) Min, J.; Kang, D. W.; Ahn, Y.-H.; Lee, W.; Cha, M.; Lee, J. W. Recoverable magnetic nanoparticles as hydrate inhibitors. *Chem. Eng. J.* **2020**, *389*, No. 124461.
(44) Demadis, K. D.; Stavgianoudaki, N.; Grossmann, G.; Gruner, M.; Schwartz, J. L. Calcium−phosphonate interactions: solution behavior and Ca^{2+} binding by 2-hydroxyethylimino-bis (methylene-phosphonate) studied by multinuclear NMR spectroscopy. *Inorg. Chem.* **2009**, *48*, 4154−4164.
(45) Pairat, R.; Sumeath, C.; Browning, F. H.; Fogler, H. S. Precipitation and Dissolution of Calcium−ATMP Precipitates for the Inhibition of Scale Formation in Porous Media. *Langmuir* **1997**, *13*, 1791−1798.
(46) (a) Lee-Steere, C. *Environmental risk assessment guidance manual for industrial chemicals*; Environment Protection and Heritage Council; Sydney (AU). [cited 2015 Dec 6], 2009. (b) Christensen, F. M.; Eisenreich, S. J.; Rasmussen, K.; Sintes, J. R.; Sokull-Kluettgen, B.; van de Plassche, E. J. European experience in chemicals management: integrating science into policy. *Environ. Sci. Technol.* **2011**, *45*, 80−89.
(47) (a) Rajković, M.; Tošković, D. V. Phosphogypsum surface characterisation using scanning electron microscopy. *Acta Period. Technol.* **2003**, *34*, 61−70. (b) Kilic, A. M.; Kilic, O. The phase transition in natural gypsum. *Asian J. Chem.* **2007**, *19*, 3157−3168.
(48) Shahid, M. K.; Choi, Y. G. The comparative study for scale inhibition on surface of RO membranes in wastewater reclamation: CO_2 purging versus three different antiscalants. *J Membr. Sci.* **2018**, *546*, 61−69.
(49) Zhu, W.; Hu, D.; Li, G.; Zheng, X. Inhibition Performance of Scale Inhibitors at Different Temperatures and Analysis of Inhibition Mechanism. *Am. Lab.* **2018**, *50*, 42−45.
(50) Amjad, Z. Inhibition of barium sulfate precipitation: effects of additives, solution pH, and supersaturation. *Water Treat.* **1994**, *9*, 47−56.
(51) Dyer, S. J.; Graham, G. M. Influence of iron on scale inhibitor performance and carbonate scale formation. In *11th NIF International Oil Field Chemical Symposium*, 2000.

https://doi.org/10.1021/acsanm.3c00445
ACS Appl. Nano Mater. 2023, 6, 6739−6750